Flow Field Prediction for Helicopter Rotor in Hover using a Vortex Embedding Method.

P. Del Bianco , E. Berton , D. Favier , C. Maresca
and W. Yonghu and J. Steinhoff

IRPHE/ASI Laboratory, UMR 6594 of CNRS, University of Aix-Marseille I & II
163 Avenue de Luminy, case 918, 13009 Marseille, France
and
Flow Analysis Incorporated. Bldg. 3
U.T.S.I- Research Park
Tullahoma TN 37388

Abstract

The present paper describes a new development of a computer code, the so called : Phoenix II, built up to predict the flowfield and the aerodynamic performance of helicopter rotors in Hover. The original numerical resolution, is based on a full potential method and allows to calculate the free convection of thin vorticals regions using a vortex embedding scheme. This modern helicopter aerodynamics approach has been recently improved and evaluated. The improvement has concerned the distribution of markers within the computational grid and the modelling of the vortical velocity in the entire domain of calculation including the immediate vicinity of the blade trailing edge. The modification of spatial weighting underrelaxation relative to the vortical component calculation has also been performed to stabilize the numerical scheme. Moreover, the axial velocities calculation has been modified by taking into account the axial velocity distribution provided at previous azimuths. The evaluation of this final code has been carried out from comparisons to experimental results obtained in the IRPHE/ASI facilities. Tests have concerned measurements of overall forces (thrust and torque), tip vortex paths, local velocities and radial distribution of circulation on model-scale of two and four bladed rotors in hover, at different pitch angles.

Nomenclature

b	Number of blades
c	Constant blade chord, (m)
C_T	Rotor thrust coefficient
C_Q	Rotor power coefficient
Γ	Blade circulation along the span, (m^2/s)
θ	Collective pitch angle at r/R=0.75, (deg)
M_{tip}	Tip mach number
r	Radial distance from the rotation axis, (m)
R	Rotor blade radius, (m)
σ	Rotor solidity ($\sigma=bc/\pi R$)
U,V,W	Radial, tangential and axial velocities, (m/s)
V_e	Rotational tip speed ($V_e = \Omega R$), m/s
Ω	Angular rotational frequency, (rad/s)
ψ	Angular blade rotation, (deg)
ρ, ρ_∞	Density, (kg/m^3)
$\vec{V}$	Total velocity, (m/s)
$\vec{q}^v$	Vortical velocity, (m/s)

Introduction

For over more than half a century, the high complexity of the flow field generated around helicopters rotors has raised a challenge for aerodynamicists. Many sophisticated experimental and computational works have been developped in order to tackle an "as good as possible" prediction of performance parameters. This effort results in new computational and experimental tools of modern helicopter aerodynamics, ranging from vortex techniques to Navier-Stokes equations resolutions, and from smoke visualisation to LDA and PIV techniques. A significant progress that emerged from this effort has been described with precision in the recent review-papers by Johnson, McCroskey, and Conlisk (Refs 1-3).

Modern aerodynamics computational methods, that have to numerically capture and structure the wake geometry and the convected vorticity, need more or less long time consuming process. A good compromise has been proposed and developed at UTSI by Steinhoff and Ramachandran (Refs 4-6). They used a full potential method for predicting hover performance with the new idea to embed the vortex structure into the flow. This vortex embedding scheme allows the free convection of thin vortical regions such as hovering rotor wakes. Nevertheless, the experimental attempt made to validate the code (Ref 7) has shown that some improvements could be carried out. The present paper gives the different changes achieved in the code, and shows the prediction efficiency obtained by comparison to experimental results.

The first part of the paper deals with the numerical methodology. The original numerical code (Phoenix II) is briefly described and the modification introduced on the trailed markers (Phoenix II-M) are presented as the first improvement. The modelling of the vortical velocity for the entire calculation domain including the region located in the immediate vicinity of the trailing edge (Phoenix II-MV) concerns the second improvement. The third improvement is obtained when taking into account the axial velocity at azimuths previously to the first blade/vortex interaction (Phoenix II-MVL).

This final code version Phoenix II-MVL is validated, in the second part of the paper, by means of experiments performed on different model scale rotors at different pitch angles. Comparisons between calculation and experiments concern overall forces (thrust and torque), tip vortex trajectories, velocity field and radial distribution of circulation.

Numerical methodology

The numerical method used in the present study is based on the full potential equation. Such a method, due to its grid dependence and to inadequate grid size, induces in regions of vorticity a rate of diffusion much faster than viscosity would suggest. To avoid this drawback, the new idea introduced by Steinhoff and Ramachandran (Refs 4-6), was to embed the vortex structure into the flow. This method (implemented in the computer code Phoenix II and called V.E for Vortex Embedding) performs the convection of thin vortical regions, as hovering rotor wake, using a lagrangian wake tracking/relaxation methods. Moreover, the compressible mass conservation equation is solved and an integral boundary-layer routine can be used to evaluate the viscous effects along the blade for power prediction. This novel approach differs from classic vortex-lattice methods by the fact that the velocity field is found using the mass conservation equation rather than the Biot-Savart law. Therefore, V.E. has the ability to compute both the free wake evolution and the inviscid compressible flow on the blade with no blade geometry modelling limitations. When combined with a boundary-layer solver this yields an ability to predict hover performance with no need of initial prescribed wake geometry or airfoil tables.

The computational method begins with the decomposition of the total velocity $\vec{V}$ into an irrotational velocity field ($\vec{\nabla}\phi$) and a rotational velocity field ($\vec{q}^{v}$), as :

$$\vec{V} = \vec{\Omega} \times \vec{r} + \vec{\nabla}\phi + \vec{q}^{v}$$

The vortical part $\vec{q}^{v}$ is concentrated near the sheet and represents the trailed circulation. $\vec{\Omega} \times \vec{r}$ results from rotational coordinates transformation.

Based on such a velocity decomposition the procedure consists in solving the steady mass conservation equation :

$$\nabla(\rho\vec{V}) = 0$$

For the resolution of the potential equation, the density ρ (normalized by the free-stream value) takes the usual isentropic form away from the sheet :

$$\frac{\rho}{\rho_\infty} = \left[1 + \left(\frac{\gamma-1}{2}\right) M_{tip}^2 \left(1 - \frac{V^2}{V_{tip}^2} \right) \right]^{\frac{1}{\gamma-1}}$$

A fixed H-grid (see Figure 1) is used to solve the compressible potential flow equation in order to determine the potential

ϕ. The vortical component $\vec{q}^{v}$ is spread over several grid points around the vortex sheet in order to concentrate the vorticity. The numerical method locates the trailed sheet by a Lagrangian convection of trailed circulation elements (markers). The circulation contained by these markers is then imposed on the flow as a $\vec{q}^{v}$ distribution (Clebsch-type).

The final result consists of an iterative process between the convection of trailed markers (convection of the shed vorticity) and the solution of the potential equation (mass conservation).

The experimental work undertaken to validate such a code (Ref 7), has nevertheless shown that some improvements remained to be performed.

A better distribution of the trailed markers : Phoenix II-M

In order to improve the prediction efficiency of the above described Phoenix II code, the first change introduced is briefly presented below and more detailed in References 7-8.

One major drawback of the numerical procedure is a trend of the markers to gather into the tip region and to be generally sparse elsewhere. The first improvement has therefore concerned the convection and the suited distribution of the trailed markers within the computational grid (code version called Phoenix II-M).

Figure 2 shows the improvement obtained from Phoenix II-M compared to Phoenix II, in the case of a four bladed rotor, nomenclatured « rotor 7 » at ASI-Laboratory (Ref 9). The bottom of the Figure gives the improvement obtained on the markers descent under the blade, and the top compares the results on CT and CQ after convergence to experimental values. It is shown that experiments are in good agreement with the improved code Phoenix II-M.

A better modelling for the vortical velocity in the very close region to the trailing edge : Phoenix II-MV

The observed discrepancies relative to the evolution of the vortex sheet, are due to an under-prediction of the vortical velocity $\vec{q}^{v}$ under the rotor disk.

To overcome this problem, the second improvement given to the code has concerned the modelling of the vortical velocity $\vec{q}^{v}$ for the entire calculation domain including the region located in the immediate vicinity of the blade trailing edge. Moreover, a modification of the weighting spatial underrelaxation relative to the vortical component calculation has been performed to stabilize the numerical scheme (code version called Phoenix II-MV). Figure 3 gives the markers positions modification, provided by the Phoenix II-M and phoenix II-MV code versions. Figure 4 clearly shows that the radial location (r/R) of the tip vortices calculated from Phoenix II-MV are in good agreement with experiments, although some discrepancies remain concerning the axial positions (z/R) in the far wake ($\Psi>2\pi/b$).

A better axial velocity distribution : Phoenix II-MVL

The azimuthal boundary conditions concerning the axial velocities calculation after the first blade/vortex interaction have been also modified to take into account the axial velocity distribution of the previous azimuths (code version called Phoenix II-MVL). The comparisons shown in Figure 4 attest a better agreement between the tip vortex trajectories calculated from Phoenix II-MVL and experiments. Nevertheless, a tendency to underpredict the far field axial convection rate is still to suffer.

Calculations using Phoenix II-MVL have been extended to a 2-blade scaled rotor with rectangular untwisted blades of symmetrical profile (« rotor 8 » in ASI nomenclature). The fixed H-grid used for the calculation is shown in Figure 5. The noteworthy modification on the markers positions is presented in Figure 6 in the case of $\theta=10°$. It can be seen from Phoenix II results (open symbols) that the markers tend to gather into the tip region, providing a lack of markers in other regions. So the first modification has concerned the convection of the trailed markers within the grid. Moreover, the vorticity contours plots have displayed the presence of two contrarotative vortices near the tip due to a too high density of markers for this azimuthal spacing. The number of azimuthal lines have then been increased in the new mesh.

Results on markers obtained when using Phoenix II-MVL (full symbols) show that the density of markers is sufficient along the span blade.

Experimental validation

In order to test Phoenix II-MVL code, the previous calculations on rotors 7 and 8 have been extended to different collective pitch angles (6 deg , 8 deg and 10 deg), and compared to experimental results performed in the ASI test facilities. The model-scale of rotor is set up on the hovering test rig installed in the hall of the S1-Luminy wind-tunnel.The model-rotor consists of a fully articuled rotor hub which can be equipped with interchangeable sets of blades.

Measurements procedures and results

Several measurements techniques suited for surveying the flow in the near and far wake regions and around the blades have been developed including X-wires anemometry and a long focal (2m to 2,5m) Laser Velocimetry (LV) technique (Refs 10-12).

Overall forces measurements (averaged thrust and torque) are performed by means of a 6-components balance mounted on the rotor hub. Tip vortex paths are measured by means of a hot-wires technique which allows the determination of the wake position as a function of the blade azimuth.

The three-dimensional velocity field around the blade is measured by a fiber optic laser velocimeter system in order to determine the circulation distribution along the blade span. In the vicinity of the blade the velocity components U,V and the axial component W are determined by LV in a fixed coordinates system. The velocities components are statistically averaged over 50 to 80 samples per azimuthal step ($\Delta\Psi$=0.72 deg). Detailed characterization of the flowfield is made possible by a combination of the .1 mm step resolution afforded by the laser optics traverse and the .3 mm diameter of the LV system measuring volume. The initiation and synchronization of the instantaneous acquisition data are realized by means of a photo-cell delivering the azimuthal origin (Ψ = 0 deg).

Figure 7 shows some examples of calculation/experiment comparisons obtained on rotor 7. The computed coefficients of thrust CT and torque CQ are compared to experimental data with a very good agreement, for three values of the collective pitch angle (see Figure 7a). Circulation distributions computed for two values of θ (8deg and 10deg) are compared to experiments performed using LV in Figure 7 b). It is shown that except at the root region of the blade, the agreement is good for both 8 deg and 10 deg. The radial location and the value of the peak of circulation is particularly well predicted. A good prediction is also shown in Figure 7 c) concerning the radial position of the tip vortex trajectory for the two values of θ. Validation on axial position of the tip vortices is less good in the far wake (Ψ>150deg), Figure 7d), as previously mentionned.

Concerning rotor 8, the same trends than previously described can be pointed out on CT, CQ and tip vortices trajectories as presented in Figure 8 for different values of the collective pitch angle.

Conclusion

The present paper has concerned a numerical investigation of the aerodynamics of a helicopter rotor in hover. An effort in improving and evaluating the capability of a vortex embedding full-potential method has been done by modifying calculation modules relative to the near and far wake geometry description and convection.
Experimental results, obtained by means of overall and local measurements focused on determining the overall airloads, the circulation distribution along the blade span and the geometry of the tip vortex path, have been used to validate this new version of the calculation model.
The present Phoenix II-MVL code has shown a good prediction efficiency in modelling the wake geometry evolution as well as local and global aerodynamic parameters, including the spanwise circulation distribution and the overall thrust and power coefficients. Improvement remains to be done concerning the tip vortex trajectory in the far wake region (Ψ>2π/b).

ACKNOWLEGMENTS

The authors wish to thank the support provided by the "Direction des Recherches Etudes et Techniques" under Grant 92/061.

REFERENCES

1 Johnson, W., "Recent Developments in Rotary Wings Aerodynamics Theory", A.I.A.A. Journal, Vol. 24, n° 8, pp. 1219-1244, August 1986.

2 McCroskey, W.J., "Some Rotorcraft Applications of Computational Fluid Dynamics", Basic Rotorcraft Research, Proceedings of 2nd International Conference, pp. 1.1-1.25, Maryland, February 1988.

3 Conlisk, A.T., "Modern Helicopter Aerodynamics", Annu. Rev. Fluid. Mech., 29, pp. 515-67, 1997.

4 Steinhoff, J. and Ramachandran, K., "Free Wake Analysis of Compressible Rotor Flows Fields in Hover", E.R.F., 12th European Rotorcraft Forum, Paper n°20, Garmish-Partenkirchen, September 1986.

5 Steinhoff, J. and Ramachandran, K., "A Vortex Embedding Method for Free Wake Analysis of Helicopter Rotor Blades in Hover", Proceedings of 13th European Rotorcraft Forum, Paper n° 11, Arles, September 1987.

6 Steinhoff, J. and Ramachandran, K., "A Vortex Embedding Method for Free Wake Analysis of Helicopter Rotor Blades in Hover", VERTICA, Vol. 13, n°2, pp. 133-141, 1989.

7 Del Bianco, P., "Contribution à l'Etude Numérique de l'Aérodynamique d'un Rotor par une Méthode de Type Potentiel Complet-Validation en Vol Stationnaire par Comparaison avec l'Expérience", Thèse de Docteur de l'Université de la Méditerranée, Université de la Méditerranée, Octobre 1996.

8 Del Bianco, P., Berton, E., Favier, D., and Maresca, "Hover Performance Prediction Using a Full Potential Method : Comparison with Experiments", in AIAA 15th Applied Aerodynamics Conference, paper 97-2323, Atlanta, June 1997.

9 Favier, D., Nsi Mba, M., Barbi, C. and Maresca, C., "A Free Wake Analysis for Hovering Rotors and Advancing Propellers", VERTICA, Vol. 11, n°3, pp. 493-511, March 1987.

10 Maresca, C., Favier, D. and Nsi Mba, M., "A Prescribed Radial Circulation Distribution of a Hovering Rotor Blade", Proceedings of 12th European Rotorcraft, Paper n° 23, Garmish-Partenkirchen, September 1986.

11 Berton, E., Favier, D., Maresca, C. and Nsi Mba, M., "A New Method of Laser Velocimetry for Airloads Determination on Hovering Rotor Blades" ICAS-AIAA, Proceedings of 19th Congress of Aeronautical Sciences, ICAS Paper n °94-353, pp. 1610-1619, Anaheim, September 1994.

12 Berton, E., Favier, D., Maresca, C. and Nsi Mba, M., "Airloads Determination on the Hovering Rotor Using a Laser Velocimetry Technique", AGARD, 75th Fluid Dynamics Panel Meeting and Symposium on Aerodynamics and Aeroacoustics of rotorcraft, AGARD CP N°. 552, Berlin, October 1994.

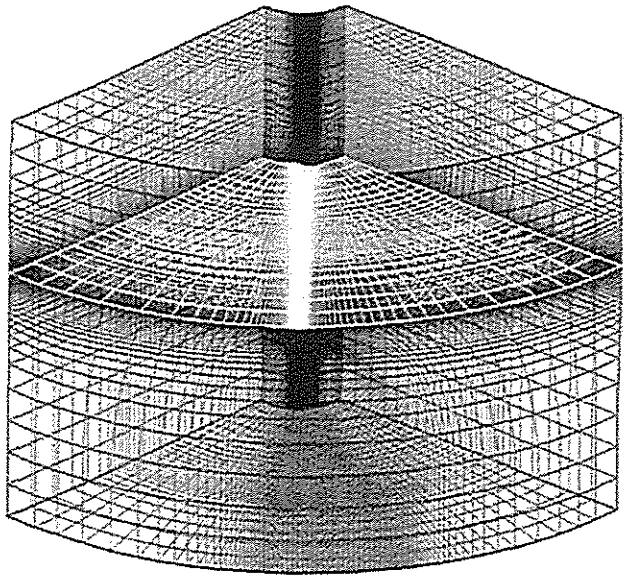

Figure 1 : Computational H-Grid.
Rotor 7, 4-blades, Collective = 10°

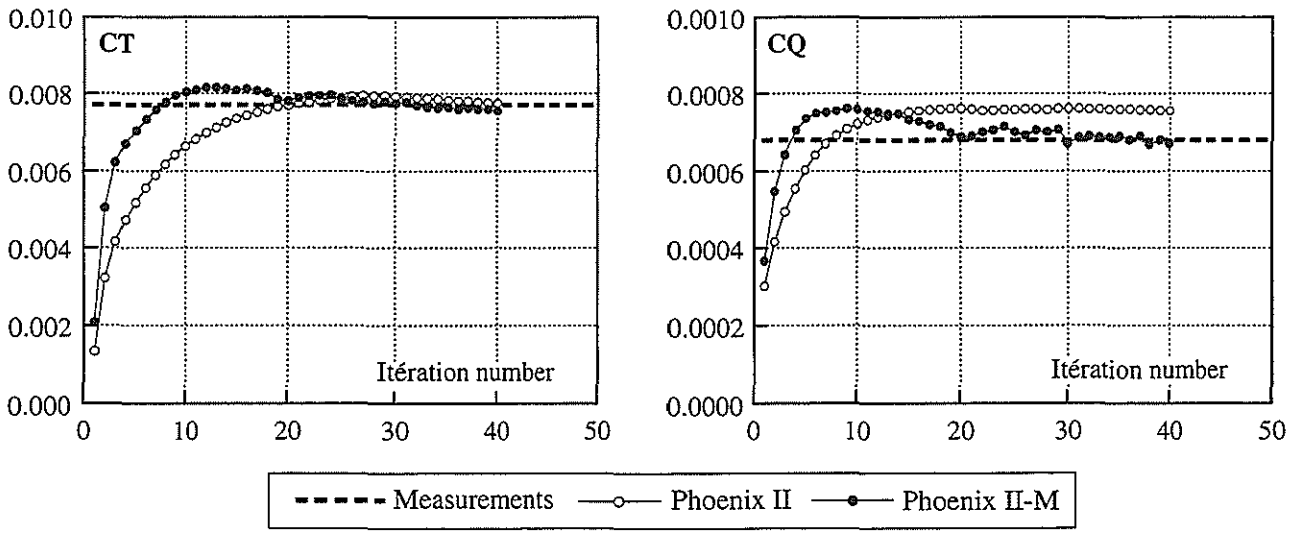

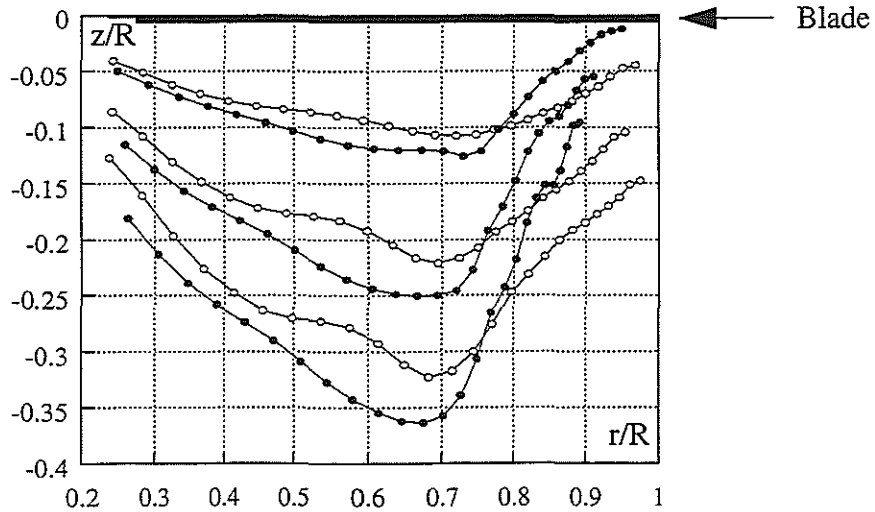

Figure 2 : Computed overall performance histories.
Rotor wake geometry (markers positions)
Rotor 7, 4-blades, Collective = 10°

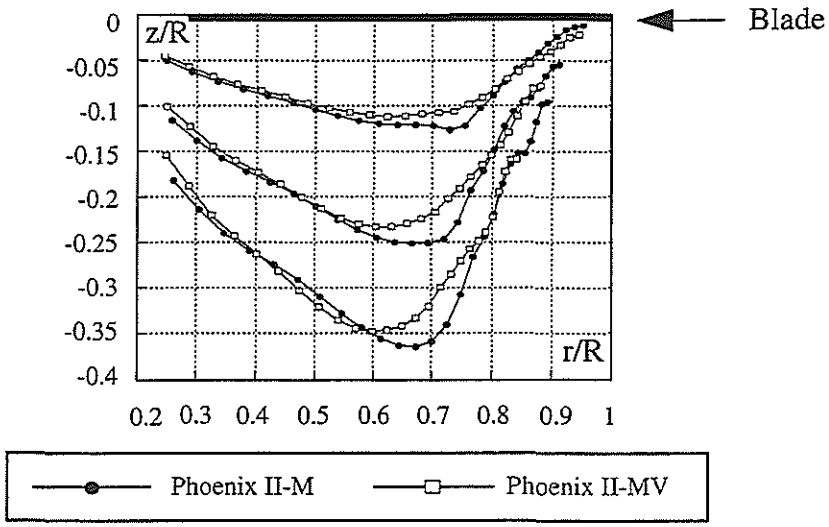

Figure 3 : Rotor wake geometry (markers positions)
Comparisons between Phoenix II-M and Phoenix II-MV
Rotor 7, 4-blades, Collective = 10°

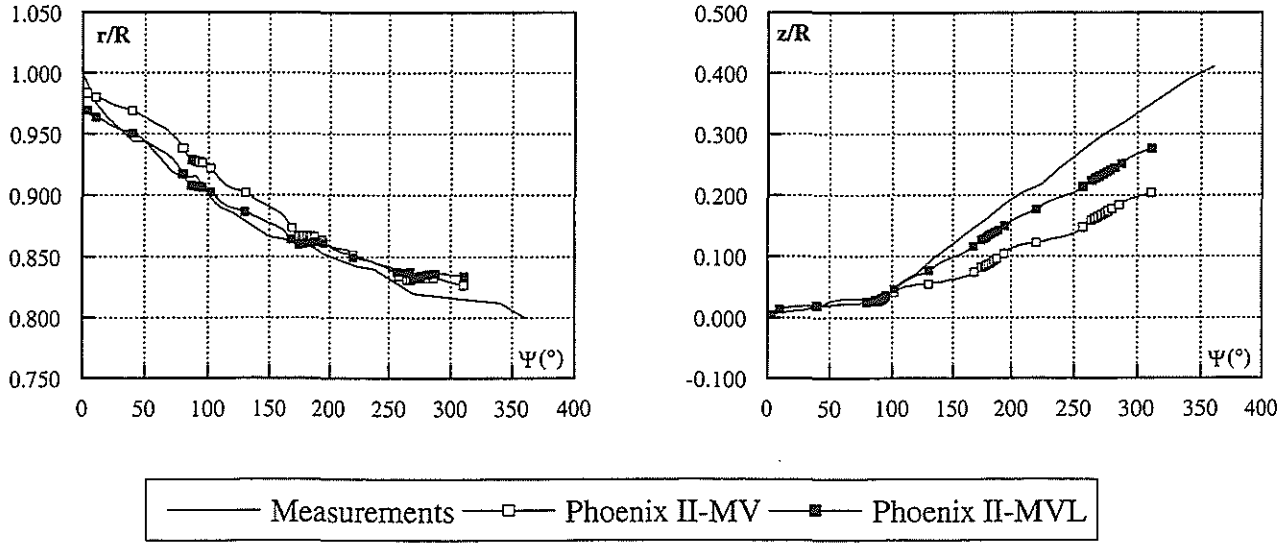

Figure 4 : Radial circulation distribution, radial and
axial convection of the tip vortex.
Rotor 7, 4-blades, Collective = 10°

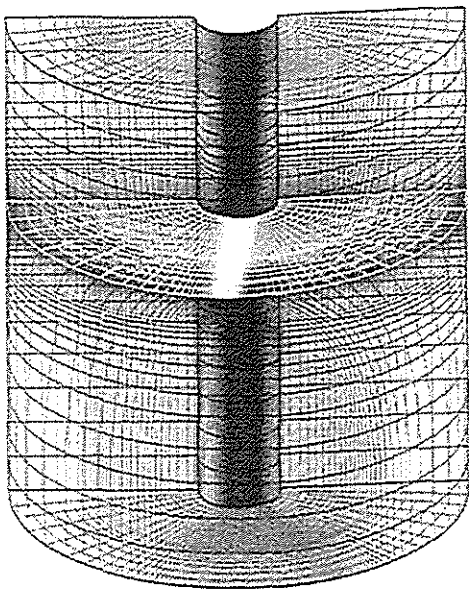

Figure 5: Computational H-grid ; Rotor 8, 2-blades, Collective = 10°

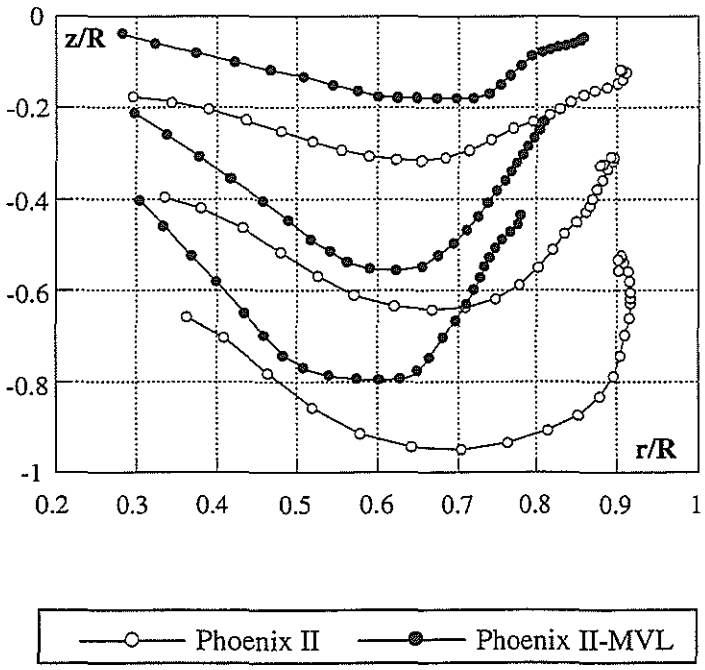

Figure 6: Rotor wake geometry (markers positions).
Rotor 8, 2-blades, collective = 10°

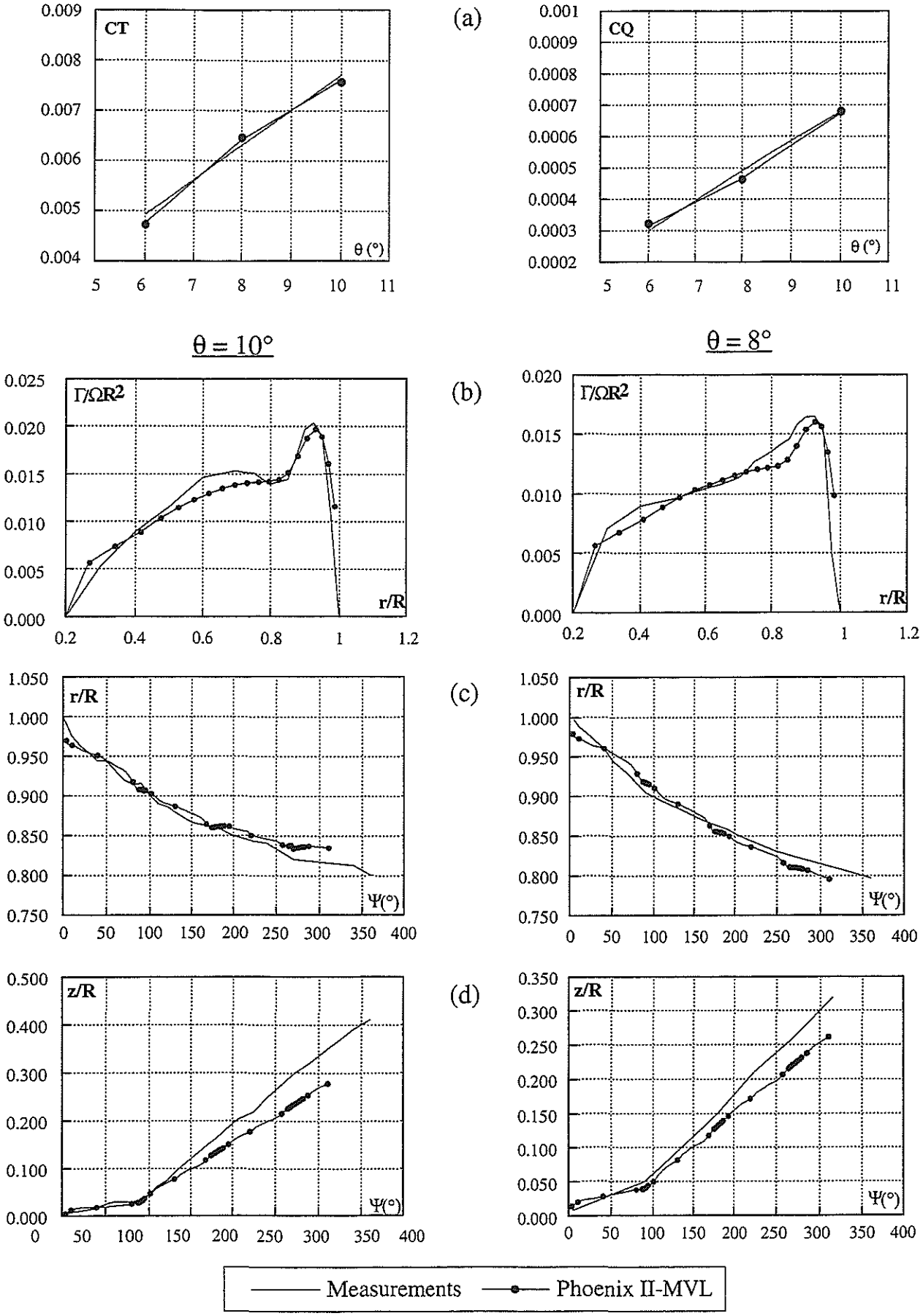

Figure 7 : Overall performance, bound circulation distribution and tip vortex trajectories
Phoenix II-MVL
Rotor 7, b=4

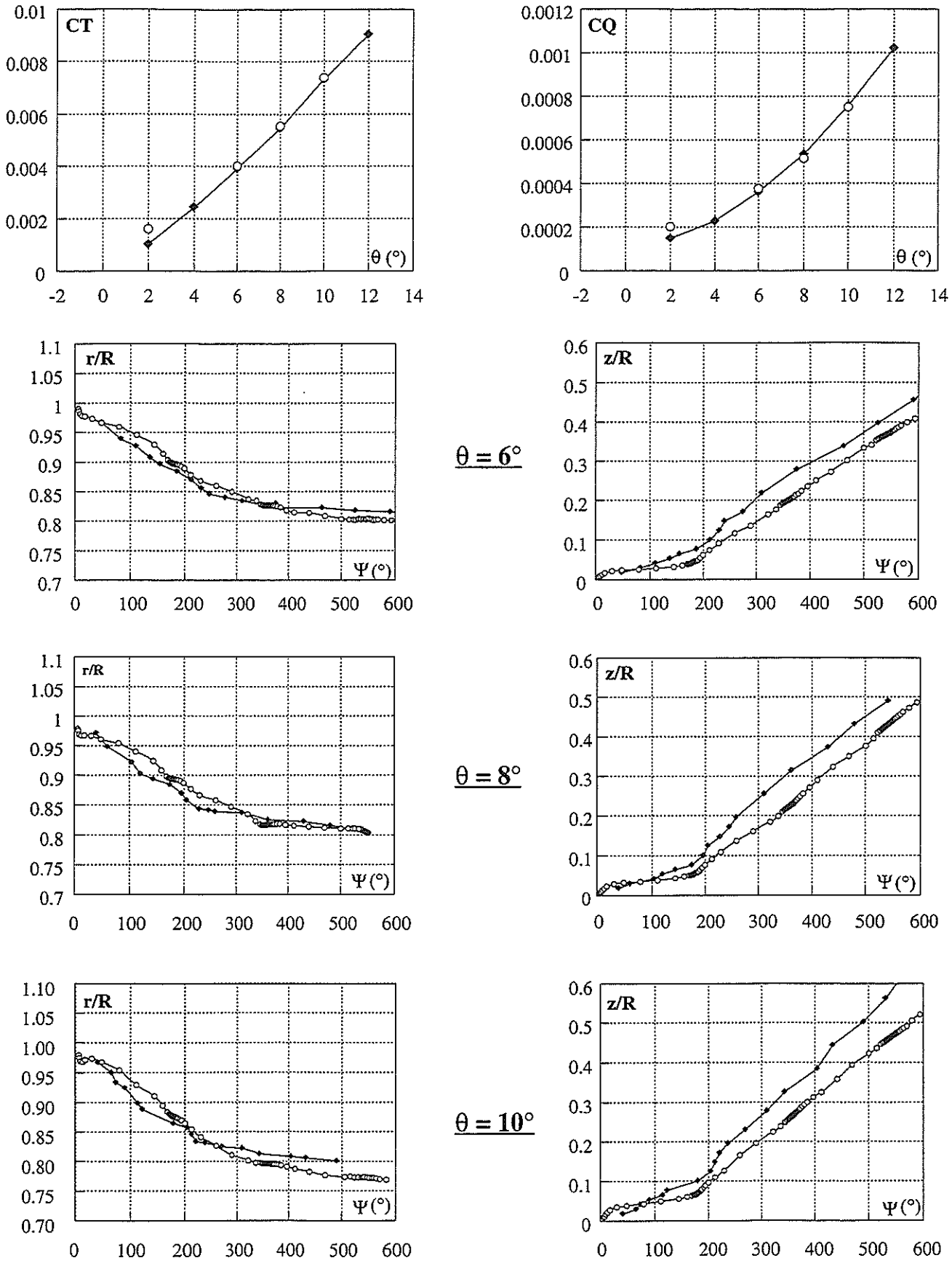

Figure 8 : Overall performance and tip vortex trajectory
Phoenix II-MVL
Rotor 8, b=2